

## LARGE LATE-TIME ASPHERICITIES IN THREE TYPE IIP SUPERNOVAE

RYAN CHORNOCK<sup>1,2</sup>, ALEXEI V. FILIPPENKO<sup>1</sup>, WEIDONG LI<sup>1</sup>, AND JEFFREY M. SILVERMAN<sup>1</sup>

*Draft version May 26, 2018*

### ABSTRACT

Type II-plateau supernovae (SNe IIP) are the results of the explosions of red supergiants and are the most common subclass of core-collapse supernovae. Past observations have shown that the outer layers of the ejecta of SNe IIP are largely spherical, but the degree of asphericity increases toward the core. We present evidence for high degrees of asphericity in the inner cores of three recent SNe IIP (SNe 2006my, 2006ov, and 2007aa), as revealed by late-time optical spectropolarimetry. The three objects were all selected to have very low interstellar polarization (ISP), which minimizes the uncertainties in ISP removal and allows us to use the continuum polarization as a tracer of asphericity. The three objects have intrinsic continuum polarizations in the range of 0.83 – 1.56% in observations taken after the end of the photometric plateau, with the polarization dropping to almost zero at the wavelengths of strong emission lines. Our observations of SN 2007aa at earlier times, taken on the photometric plateau, show contrastingly smaller continuum polarizations ( $\sim 0.1\%$ ). The late-time H $\alpha$  and [O I] line profiles of SN 2006ov provide further evidence for asphericities in the inner ejecta. Such high core polarizations in very ordinary core-collapse supernovae provide further evidence that essentially all core-collapse supernova explosions are highly aspherical, even if the outer parts of the ejecta show only small deviations from spherical symmetry.

*Subject headings:* polarization — supernovae: individual (SN 2006my, SN 2006ov, SN 2007aa)

### 1. INTRODUCTION

Core-collapse supernovae (SNe) are the explosive deaths of massive stars. Indirect inferences that these energetic explosions are aspherical have come from such evidence as the high space velocities of the pulsars produced by the SNe (Lyne & Lorimer 1994) and the structure of Galactic supernova remnants (e.g., Fesen 2001). A direct observational test for the presence of asphericity in SNe was proposed by Shapiro & Sutherland (1982), who pointed out that the polarizing effects of electron scattering in a supernova atmosphere would not cancel if the supernova were aspherical and spatially unresolved by a distant observer.

The first published detections of supernova polarization were for SN 1987A (Barrett 1988; Cropper et al. 1988; Mendez et al. 1988). Subsequent observations of additional SNe led to the discovery that all core-collapse supernovae with data of sufficient quality exhibit polarization, as recently reviewed by Wang & Wheeler (2008). An important test of our understanding was provided by the late-time *Hubble Space Telescope* (*HST*) images of SN 1987A which spatially resolve the ejecta and show that they are elongated along a position angle (P.A.) consistent with that inferred from the polarimetry (Wang et al. 2002).

Our study here focuses on SNe IIP, which represent the single most common outcome for the ends of the lives of massive stars. Approximately 50% of all core-collapse SNe are of this subtype (Li et al., in prep.; see also Smartt et al. 2009). Their progenitors are relatively low-mass red supergiants in the mass range of

8.5–16.5  $M_{\odot}$  (Smartt et al. 2009) that are either isolated or sufficiently separated from their binary companions so as to leave their evolution and outer envelopes unaffected (Heger et al. 2003; Li et al. 2006; Smartt et al. 2009). In many ways, their progenitors and explosions should be the simplest ones to understand and model.

Despite this, published spectropolarimetry of SNe IIP is surprisingly limited. Most of the objects of this type listed in the compilation of Wang & Wheeler (2008) as having available polarimetry are either unpublished or have only photometric polarimetry. Our focus here is on measuring continuum polarization and separating intrinsic continuum polarization from the effects of interstellar polarization (ISP); with only photometric data, this is extremely difficult, if not impossible.

The two SNe IIP that have been the most well-studied spectropolarimetrically are SNe 1999em and 2004dj. SN 1999em showed low polarization shortly after explosion, indicating that the outer ejecta were nearly spherical. The level of continuum polarization slowly increased with time in a manner consistent with a single axis of symmetry while simultaneously the polarization signatures in the lines grew (Leonard et al. 2001; Wang & Wheeler 2008). SN 2004dj showed no detectable polarization (after correction for ISP) in the continuum or lines while on the plateau. At the end of the plateau stage, the continuum polarization jumped up to 0.56%, revealing an aspherical core (Leonard et al. 2006). The polarization percentage slowly decreased thereafter in a manner attributed to geometric dilution of the scattering electrons as the ejecta expanded. The observations of SN 2004dj prompted the present study in an attempt to determine whether the results for SN 2004dj were common to SNe IIP.

Three recent SNe IIP in the Virgo Cluster have provided an opportunity to study this class of objects in more detail. SN 2006my was discovered by K. Itagaki

<sup>1</sup> Department of Astronomy, University of California, Berkeley, CA 94720-3411, USA.

<sup>2</sup> Current address: Harvard-Smithsonian Center for Astrophysics, 60 Garden Street, Cambridge, MA 02138, USA, rchornock@cfa.harvard.edu.

in NGC 4651 on 2006 November 8.82 (UT dates are used throughout this paper; Nakano & Itagaki 2006a). The same observer also discovered SN 2006ov in M61 on 2006 November 24.86 (Nakano & Itagaki 2006b). Both objects were soon spectroscopically confirmed as SNe IIP a few months past explosion (Stanishev & Nielsen 2006; Blondin et al. 2006). SN 2007aa in NGC 4030 was discovered by T. Doi on 2007 February 18.308 and spectra obtained by N. Morrell on Feb. 19.24 showed that it was a SN IIP similar to SN 1999em at about 20 days after explosion (Doi 2007; Folatelli & Morrell 2007). Li et al. (2007) presented photometric and spectroscopic evidence that both SN 2006my and SN 2006ov were normal Type IIP SNe discovered near the end of the photometric plateau stage.

While Li et al. (2007) identified possible progenitors for SNe 2006my and 2006ov in pre-explosion *HST* images, subsequent work has rejected those identifications (Leonard et al. 2009; Smartt et al. 2009; Crockett et al. 2009). Instead, Smartt et al. (2009) and Crockett et al. (2009) give upper limits for the zero-age main-sequence masses of any progenitor in the *HST* images of 13, 10, and 12  $M_{\odot}$  for SNe 2006my, 2006ov, and 2007aa, respectively. Smartt et al. (2009) also quote values for the  $^{56}\text{Ni}$  masses produced by SN 2006ov and SN 2006my of  $0.003 \pm 0.002 M_{\odot}$  and  $0.03 \pm 0.015 M_{\odot}$ , respectively, based on analyses of the late-time light curves. The  $^{56}\text{Ni}$  mass inferred for SN 2006ov is extremely low, comparable to that of the underluminous SN 1999br (Hamuy 2003; Pastorello et al. 2004), despite SN 2006ov having a normal luminosity on the plateau.

In this paper, we present spectropolarimetry of the above three SNe IIP obtained after the end of the photometric plateau. In §2, we describe the observations and corrections for small amounts of ISP from the Galaxy. We present the evidence for very high intrinsic continuum polarizations in these objects in §3 and discuss the interpretation and implications of our results in §4.

## 2. OBSERVATIONS

Unfiltered images of all three SNe in our sample were obtained as part of our regular monitoring of their host galaxies for the Lick Observatory Supernova Search using the 0.76-m Katzman Automatic Imaging Telescope (KAIT; Filippenko et al. 2001), although we artificially increased the frequency of observations from the default search strategy to better sample the light curves of these objects. Portions of the SN 2006ov and SN 2006my light curves have already been presented and the reductions described by Li et al. (2007). Briefly, a point-spread function fitting technique was used to subtract pre-SN template images from the SN observations and aperture photometry was performed on the subtracted images using DAOPHOT (Stetson 1987) in IRAF<sup>3</sup>. KAIT unfiltered observations approximate the standard *R* band (Li et al. 2003), so the SN observations were then calibrated to an average of USNO-B1 stars in the field (up to 20 per field), resulting in systematic uncertainties in the zero points for each field of 0.05 – 0.18 mag. However,

only the shapes of the light curves are relevant for this study.

We obtained spectropolarimetry of the three SNe using both the Kast spectrograph on the Lick 3-m Shane telescope (Miller & Stone 1993) and the Low Resolution Imaging Spectrometer (LRIS) mounted on the Keck I 10-m telescope (Oke et al. 1995). The Kast data were obtained using the red camera only, with the 300/7500 grating tilted to cover a wavelength range of approximately 4400–9900 Å in conjunction with a GG455 order-blocking filter. A small amount of second-order light is likely present at wavelengths greater than  $\sim 9000$  Å, but none of our conclusions depend on data at those wavelengths. A 3''-wide slit gave a spectral resolution of  $\sim 16$  Å.

The LRIS data were taken with both halves of the spectrograph. All observations used an identical setup with the D560 dichroic beam-splitter to split the spectrum near 5500 – 5600 Å, along with the 600/5000 grism on the blue side and the 400/7500 grating on the red side. We used a 1''5-wide slit to achieve spectral resolutions of  $\sim 6$  Å and 9 Å on the blue and red sides, respectively. The total spectral coverage was 3170 – 9240 Å, but the polarization data plotted in this paper are typically truncated below  $\sim 4000$  Å because the low blue flux in SNe IIP due to line blanketing, and decreasing detector sensitivity at short wavelengths, combine to make the polarimetry extremely noisy at the blue end. In addition, this spectral region suffers from background-subtraction uncertainties due to the underlying blue starlight from the host galaxy. Further details of the individual observations are given in Table 1.

Basic two-dimensional image processing and spectral extraction were accomplished using standard tasks in IRAF. Flux calibration and removal of atmospheric absorption bands (Wade & Horne 1988) was performed using our own IDL tasks (Matheson et al. 2000). The individual one-dimensional SN spectra were combined on a pixel-by-pixel basis, weighted using the error estimates from the optimal spectral extraction technique (Horne 1986), and the final blue-side and red-side spectra (for LRIS) were scaled and combined across the overlap region. In those cases where differential loss of blue light was apparent because the observed P.A. of the observations deviated from the parallactic angle (Filippenko 1982), the combined observation was warped to the shape of the observation obtained closest to the parallactic angle using a low-order polynomial fit to the ratio of the spectra.

We also extracted some of the emission from nearby H II regions along the slits of selected observations. We fit Gaussians to the nebular emission lines and obtained recession velocities of 920, 1660, and 1650  $\text{km s}^{-1}$  for the H II regions near SN 2006my, SN 2006ov, and SN 2007aa, respectively. These values are within a typical value for a galactic rotation velocity (100 – 200  $\text{km s}^{-1}$ ) of those listed for the host-galaxy nuclei in the NASA Extragalactic Database (NED), so we adopt these redshifts in this paper and have removed them from all plots. All references to wavelengths are in the rest frame of each object.

### 2.1. Spectropolarimetry

The spectropolarimetric observations were reduced following the standard method of Miller et al. (1988), as

<sup>3</sup> IRAF is distributed by the National Optical Astronomy Observatories (NOAO), which are operated by the Association of Universities for Research in Astronomy, Inc., under cooperative agreement with the National Science Foundation.

TABLE 1  
DETAILS OF OBSERVATIONS

Object	UT Date (YYYY MM DD.DD)	Age <sup>a</sup> (d)	Telescope <sup>b</sup>	Total Exposure Time (s)	Seeing ( $''$ )	P.A. ( $^{\circ}$ )	Notes
SN 2006ov	2006 12 20.51	-5	L3	4800	2.2	144.5	clouds
SN 2006ov	2006 12 25.63	0	K1	4000	1.4	125	clear
SN 2006ov	2007 01 21.56	27	K1	4400	0.8	125	clear
SN 2006my	2007 01 21.50	38	K1	3600	0.9	282	clear
SN 2007aa	2007 03 18.45	-50	K1	3600	1.0	359.7	clear, poor guiding
SN 2007aa	2007 04 15.48	-22	K1	2800	1.8	57.5	clear
SN 2007aa	2007 05 10.31	3	L3	7200	2.1	203	clear

<sup>a</sup> Age relative to the end of the plateau,  $t_p$  (see §3 for a definition).

<sup>b</sup> L3 = Lick 3-m + Kast spectrograph; K1 = Keck I 10-m + LRISp.

implemented by Leonard et al. (2001). The angle zero points of the waveplates were determined using polarimetric standards from Schmidt et al. (1992). Typically, two standards were observed per night to confirm the zero point. In addition, we noted that the zero points for each instrument were generally stable over time with small shifts. Low-polarization standards from the literature (Mathewson & Ford 1970; Clemens & Tapia 1990; Schmidt et al. 1992; Berdyugin et al. 1995) were observed on each night to have negligible polarizations, setting a limit on the instrumental polarization of  $P < 0.1\%$ .

This study hinges on our ability to accurately measure the continuum polarization of SNe. ISP in both our own Galaxy and the host galaxies of these SNe can mimic the presence of continuum polarization and contaminate our results. All three SNe selected for this study are at high Galactic latitudes ( $b > 59^{\circ}$ ) and hence low Galactic ISP is expected (Serkowski et al. 1975) based on the low columns ( $E(B - V) < 0.03$  mag) measured along these lines of sight (Schlegel et al. 1998). We can directly measure the Galactic contribution to the ISP by following the lead of Tran (1995a) and selecting stars of low intrinsic polarizations and sufficiently large distances (estimated via spectroscopic parallaxes) to place them out of the Galactic plane. Such probe stars should sample most of the Galactic contribution to the ISP along these lines of sight. The probe stars for SN 2006my were BD +17 $^{\circ}$ 2526 and BD +16 $^{\circ}$ 2409, those for SN 2006ov were BD +05 $^{\circ}$ 2618 and BD +04 $^{\circ}$ 2608, while BD +00 $^{\circ}$ 2876 and BD -00 $^{\circ}$ 2514 were selected for SN 2007aa.

The probe stars were observed immediately after the object on one observation date per SN with the slit kept at the same P.A. Each pair of stars gave consistent results (within 0.1% in each Stokes parameter), so the two stars were averaged to form our estimate of the Galactic ISP for each SN. As expected, the Galactic ISPs were very small, with  $V$ -band polarizations of 0.07%, 0.06%, and 0.16% measured for the SN 2006my, SN 2006ov, and SN 2007aa probes, respectively. For the sake of completeness, we subtracted low-order polynomial fits to the Stokes  $q$  and  $u$  of the combined probes from the Stokes parameters measured during each SN observation, although the effect is almost negligible for SN 2006my and SN 2006ov.

As a final check on our instrumental stability, we observed the same probe star, BD +05 $^{\circ}$ 2618, on all three occasions that we obtained spectropolarimetry of SN 2006ov. The variation in each Stokes parameter

was  $< 0.04\%$ , consistent with similar experiments we have performed in the past with repeated observations of bright stars on different nights. This sets an upper limit to any systematic offset between the Lick and Keck polarimeters as well as to any night-to-night instrumental instability. We note that Leonard et al. (2006) also found similar results using the Kast polarimeter. Therefore, we adopt a value of 0.04% for any systematic error contribution where appropriate in the analysis below.

### 3. RESULTS

As shown by Li et al. (2007) for SN 2006my and SN 2006ov, and below for SN 2007aa, all three objects in our study exhibit standard light-curve shapes for SNe IIP, with the three phases of a relatively flat plateau followed by a rapid decline phase and then a steady decline at a rate consistent with the radioactive decay of  $^{56}\text{Co}$ . This characteristic shape is well understood theoretically (Eastman et al. 1994; Kasen & Woosley 2009) and defines this subclass of SNe (Barbon et al. 1979; Doggett & Branch 1985). The supernova shock deposits thermal energy in the envelope which is released as the hydrogen in the envelope recombines during the plateau phase. When the photosphere recedes all the way back through the hydrogen layer, recombination ceases to be a source of energy and the SN light curve rapidly falls until the luminosity matches the instantaneous rate of energy input from the decay of  $^{56}\text{Co}$ .

Both SN 2006my and SN 2006ov were discovered several months after explosion near the ends of their plateaus. In order to make temporal comparisons amongst our observations of these SNe when the dates of explosion are so poorly known, we found it convenient to define a common time to represent the end of the plateau. As discussed below, the timing relative to the end of the plateau is probably the important physical parameter for the polarization, not the time elapsed since explosion.

Hamuy (2003) defined the end of the plateau phase,  $t_p$ , as the time when the SN magnitude falls halfway between its value on the plateau and the value at the start of the radioactive decay tail. The plateau magnitude can be difficult to uniquely define in some cases due to the varied shapes of SN IIP light curves. The compilation of SN IIP photometry by Poznanski et al. (2009) shows that some objects have ‘‘plateau’’ phases that actually rise for many days before falling while others steadily, if slowly, decline from the beginning. The photometric band used to define the light curve can also have an effect as the shapes of SN IIP light curves are a function of

wavelength. Hamuy (2003) used the  $V$  band, but we have only unfiltered photometry for our three objects.

Despite these uncertainties in the definition of the plateau magnitude,  $t_p$  occurs during the rapid decline phase and hence the uncertainty in  $t_p$  is at worst a few days, which is negligible for our purposes. We measure dates for  $t_p$  of 2006 Dec. 15.0, 2006 Dec. 25.5, and 2007 May 7.3 for SNe 2006my, 2006ov, and 2007aa, respectively, based on the KAIT unfiltered photometry. Below, we measure  $t_p$  for SN 1999em in the  $R$  band (which most closely approximates our KAIT unfiltered photometry), and our value for  $t_p$  differs by only 0.2 days from the value derived by Hamuy (2003) in  $V$ , so we can conclude that bandpass effects have negligible effect on our measured values for  $t_p$ . Hereafter, dates listed as “day X” refer to epochs of observation X days after the end of the plateau as defined by  $t_p$ .

Li et al. (2007) found that SN 2006my and SN 2006ov were not highly reddened and had no detectable Na I D absorption lines from the interstellar media of their hosts. We confirm the lack of narrow Na I absorption in our spectra. Our highest signal-to-noise ratio (S/N) spectra of each object are plotted in Figure 1. SN 2007aa does have a weak dip near 5888 Å that may be from absorption in NGC 4030. The strength of the feature in SN 2007aa is difficult to quantify at our low spectral resolution, especially with the curvature of the spectrum making the continuum hard to define. We estimate the equivalent width of the dip to be  $\sim 0.08$  Å, with an uncertainty of about 50%. If two-thirds of the absorption is due to the D1 component of the doublet (reflecting the ratio of the oscillator strengths, as expected in the low optical depth limit), the relationship of Munari & Zwitter (1997) predicts a host-galaxy reddening of  $E(B - V) \approx 0.014$  mag, which corresponds to an ISP of  $P \approx 0.04\%$  for typical lines of sight in the Galaxy, up to an empirical maximum of  $P \approx 0.13\%$  (Serkowski et al. 1975). SNe 2006my and 2006ov appear to have even less absorption from their host galaxies. Even if our estimates of the reddening are off by a factor of a few, the conclusion that we should expect our objects to have low host-galaxy ISP will be unchanged.

### 3.1. SN 2006ov

We obtained three epochs of spectropolarimetry on SN 2006ov, two during the steep fall off the photometric plateau and one a month later. Our highest S/N data were obtained from Keck on day 0 and were fortuitously exactly synchronized with the end of the plateau. These data are plotted in the  $q - u$  plane in Figure 2, with each black circle representing a 100 Å bin of data. As described above, the S/N degrades to the blue, so we only plot data at wavelengths greater than 4500 Å. The cloud of points is clearly elongated in the positive  $q$ , positive  $u$  direction by an amount in excess of the error bars, indicating substantial intrinsic supernova polarization.

We selected two broad wavelength intervals, 6800–7200 and 7820–8140 Å, as representative of the line-free continuum (the exact choice is justified below) and plotted the integrated polarizations<sup>4</sup> as the blue diamond and

<sup>4</sup> All integrated polarizations in this paper are calculated from the flux-weighted averages of  $q$  and  $u$  over the indicated wavelength intervals.

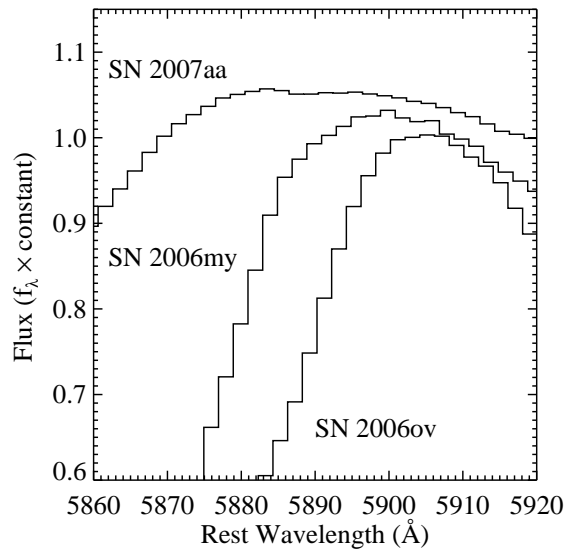


FIG. 1.— The spectral region near the Na I  $\lambda\lambda 5890, 5896$  doublet for each of the three SNe. The plotted spectra are from days 38, 0, and  $-50$  for SNe 2006my, 2006ov, and 2007aa, respectively. SN 2007aa shows a tiny dip near 5888 Å that may be Na I absorption in its host galaxy. The other two SNe show even less evidence for host-galaxy absorption, indicating that we should expect negligible ISP from the host galaxies of these objects.

solid red circle in Figure 2. The two continuum points are very consistent with each other and have an average polarization (weighted by the inverses of their variances) of  $P = 1.56 \pm 0.03\%$  at P.A. =  $8^\circ 2 \pm 0^\circ 6$ . Many of the 100 Å bins of data are clustered around these continuum points and along the line connecting them to the origin. The P.A. of  $8^\circ 2$  therefore is significant in this object and probably represents the projection of the SN symmetry axis onto the plane of the sky. Since the Stokes parameters ( $q, u$ ) are referenced to the arbitrary direction of North on the sky, it is useful to rotate our coordinate system to align one Stokes parameter with the symmetry axis of the SN. We call these new coordinates rotated Stokes parameters (RSP; Trammell et al. 1993a; Tran 1995b). If the SN were axisymmetric,  $q_{\text{RSP}}$  would be an estimator of the total polarization and  $u_{\text{RSP}}$  would show any deviations from axisymmetry.

The polarization data after rotation are plotted in Figure 3 in 20 Å bins. The most striking aspect of Figure 3 is the high level of polarization ( $P \approx 1.5\%$ ) in the continuum, with many strong, sharp depolarizations down to almost zero in  $q_{\text{RSP}}$  present at the lines. We integrated the polarimetry over the wavelength range 6540–6600 Å to determine the polarization at the peak of H $\alpha$  and measured  $(q_{\text{RSP}}, u_{\text{RSP}})$  of (0.08%, 0.00%), with error bars of 0.05% in each Stokes parameter. The similar depolarizations present for many other lines are convincing evidence that the host-galaxy contribution to the ISP must be very small ( $\lesssim 0.1\%$ ), as might be expected from the low reddening to SN 2006ov. To estimate the ISP, many past workers have made the assumption that the intrinsic polarization in supernovae at the peaks of strong lines is zero (Trammell et al. 1993b; Höflich et al. 1996; Tran et al. 1997), but that assumption is clearly wrong in some cases (Maund et al. 2007b), especially at early times when He I  $\lambda 6678$  is blended with H $\alpha$ . Here, the continuum polarization we measure must be almost entirely intrinsic to SN 2006ov and the lines are in fact

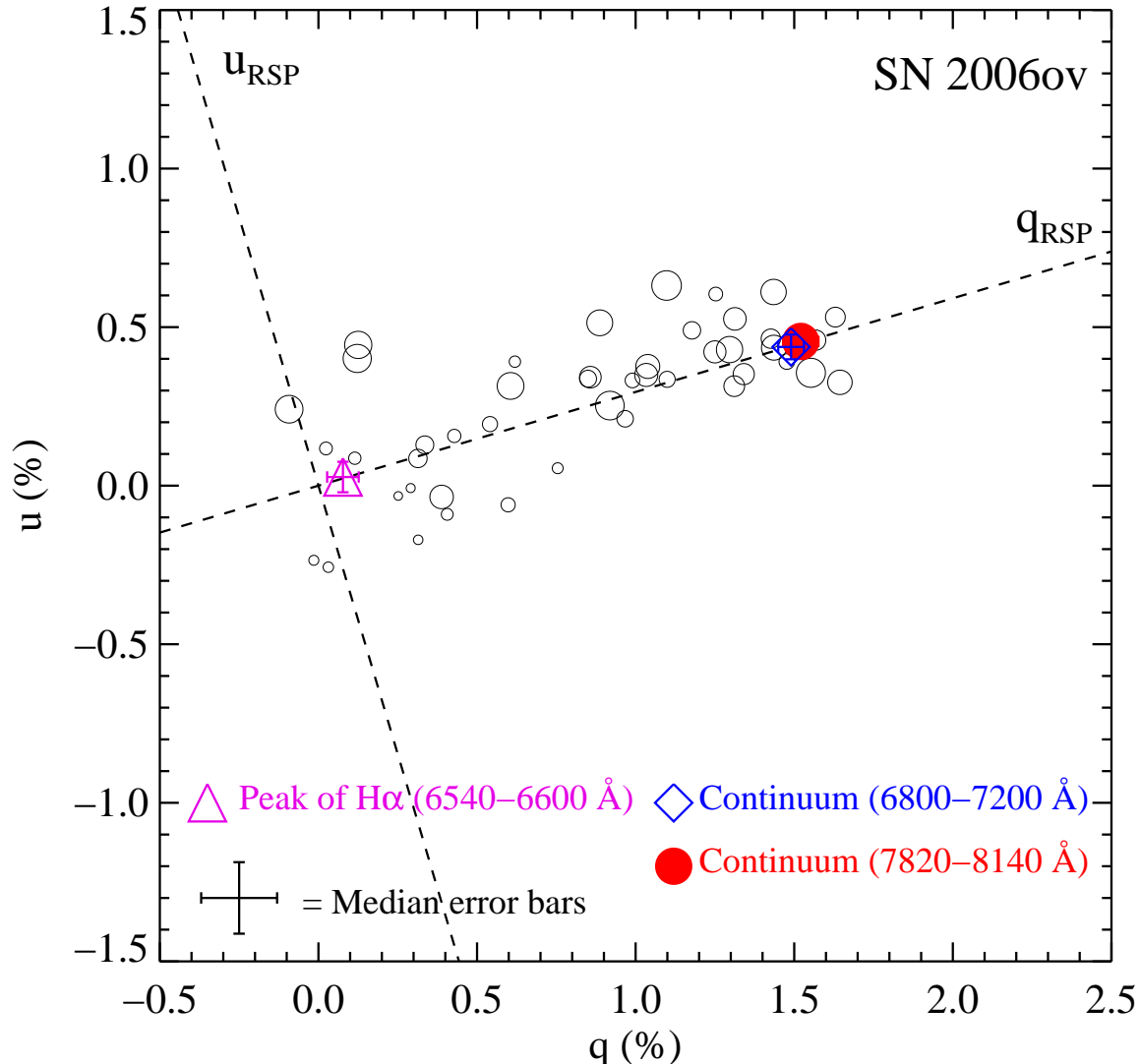


FIG. 2.— SN 2006ov data from 2006 Dec. 25 (day 0) plotted in the  $q - u$  plane. The black circles represent 100 Å bins of data at wavelengths greater than 4500 Å. The radii of the circles are proportional to wavelength. The blue diamond and solid red circle represent the polarization in two continuum bins while the purple triangle marks the peak of the  $H\alpha$  emission line. The dashed lines represent the preferred, rotated set of Stokes parameters  $q_{\text{RSP}}$  and  $u_{\text{RSP}}$ , chosen to align  $q_{\text{RSP}}$  with the two continuum bins. The cross at  $(-0.25, -1.3)$  shows the size of the median error bars on the data points.

depolarized.

With that in mind, we can now justify our choice of continuum intervals plotted in Figure 2 and marked on Figure 3. Past work has noted the utility of measuring the continuum polarization in the red portion of the optical where few line features interfere with the measurement. Leonard et al. (2006) used a wide continuum region of 6800–8200 Å in their study of SN 2004dj. Integrating the observed polarization over a continuum region that wide for SN 2006ov will clearly underestimate the true polarization as it will include a strong depolarization present at the K I/O I blend as well as a weaker one due to [Ca II] emission. We formally get  $P = 1.26 \pm 0.02\%$  if we use the wide definition for the continuum, significantly less than the value of 1.56% quoted above. Therefore, we define two continuum regions to exclude the strong lines. The first one, 6800–7200 Å, is designed to avoid the red wing of  $H\alpha$  at its blue end and

also exclude the [Ca II] emission at the red end. The second region, 7820–8140 Å, is bracketed by O I  $\lambda 7774$  and Na I  $\lambda\lambda 8183, 8194$ .

We also obtained SN 2006ov data on two additional epochs, days  $-5$  and 27. We have plotted a comparison of  $q_{\text{RSP}}$  on all three epochs in Figure 4. Due to the lower S/N of the additional data, we have rebinned to 50 Å per pixel. Despite the significant noise, the overall pattern is the same: large continuum polarization with dips down to nearly zero present at the wavelengths of strong line features. The Lick data were taken only 5 days before the day 0 Keck data and do show some significant differences, indicating rapid evolution of the spectrum as the SN made the transition off the photometric plateau. For example, the depolarizations in the wavelength range 6000–6500 Å are more blended together at day  $-5$  than at day 0.

We calculated the polarization in both of our contin-

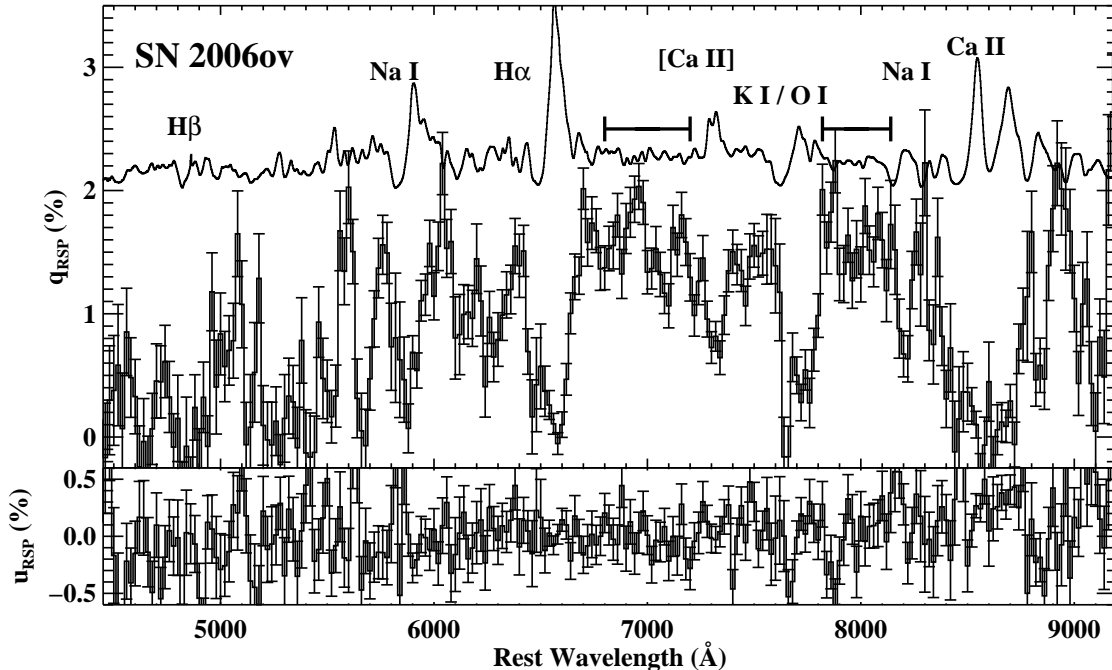


FIG. 3.— Spectropolarimetry of SN 2006ov on day 0, presented as 20 Å bins in the rotated  $q_{\text{RSP}}-u_{\text{RSP}}$  coordinate system so that  $q_{\text{RSP}}$  is an estimator of the polarization and  $u_{\text{RSP}}$  is near zero. The total-flux spectrum of SN 2006ov is overplotted in the top panel to guide the eye, with several major lines labeled. The continuum polarization between strong line features is very high ( $\sim 1.5\%$ ), but the lines result in depolarization. The two horizontal black bars mark the extent of our two relatively line-free regions (6800–7200 and 7820–8140 Å), which we take to be representative of the continuum.

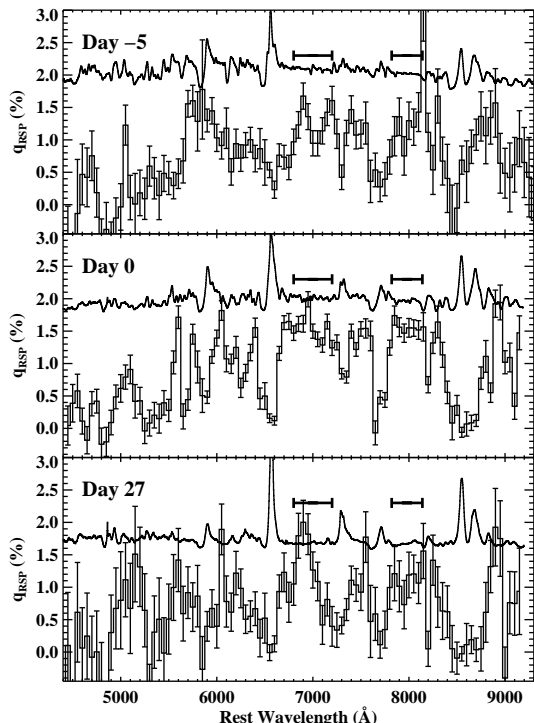


FIG. 4.— Three epochs of polarization data for SN 2006ov. The data points with error bars represent the Stokes parameter  $q_{\text{RSP}}$ , which is an estimator of the total polarization. As a reference, the solid line in each figure is the total-flux spectrum from each epoch. Note the high continuum polarization, with depressions at the location of the strong lines. The high point near 8150 Å in the day  $-5$  polarization is spurious and due to relatively poor night-sky subtraction. The two horizontal black bars mark our two continuum regions.

um regions for each of our three epochs. The results are plotted in Figure 5 and compared to the KAIT unfiltered light curve. The two continuum windows gave very consistent results, showing a significant increase in the weighted-average polarization in only five days, from  $1.25 \pm 0.06\%$  on day  $-5$  to  $1.56 \pm 0.03\%$  on day 0, falling to  $1.15 \pm 0.08\%$  on day 27. SN 2004dj showed large variations in the polarization angle at the end of the plateau (Leonard et al. 2006), but the SN 2006ov continuum observations are consistent with a single P.A. to within  $1^\circ$ . Unfortunately, SN 2006ov exploded while in solar conjunction and we were unable to obtain observations in the month between discovery and our day  $-5$  data, so it was impossible to establish whether the high polarization apparent at late times represented a significant change from early times.

### 3.2. SN 2006my

We obtained a single epoch of spectropolarimetry of SN 2006my on day 38, 2007 Jan. 21. We analyzed the data in a similar manner to SN 2006ov above. First, we measured the weighted average polarization in our two continuum windows to be  $P = 0.97 \pm 0.04\%$  at P.A. =  $174^\circ \pm 1^\circ$ . Then we rotated our Stokes parameters by  $174^\circ$  to align  $q_{\text{RSP}}$  with this polarization angle. The results are plotted in Figure 6.

The data are of lower quality than for SN 2006ov but show broadly similar characteristics. High continuum polarization is seen in  $q_{\text{RSP}}$ , with deep depolarizations present at the wavelengths of strong line features. Li et al. (2007) found that the extinction to SN 2006my was likely to be minimal, and hence low ISP should be expected. We determined the polarization at the peak of H $\alpha$  using the same window as for SN 2006ov above and found  $(q_{\text{RSP}}, u_{\text{RSP}})$  of  $(0.03\%, 0.03\%)$  with an un-

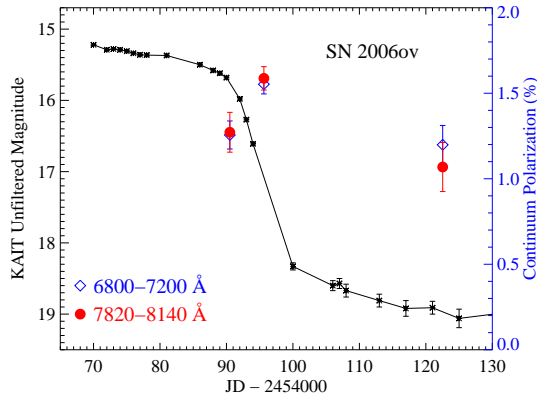


FIG. 5.— Continuum polarization evolution in SN 2006ov. The black stars are the KAIT unfiltered light curve of SN 2006ov, with the solid line connecting the points to guide the eye. The blue diamonds and solid red circles represent the polarization in our two continuum windows. The end of the plateau,  $t_p$ , corresponds to  $\text{JD} = 2454095$ . The plotted error bars on the polarizations include a 0.04% systematic error contribution. The two horizontal black bars mark our two continuum regions.

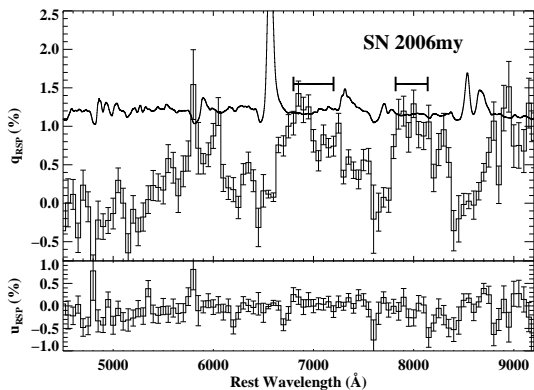


FIG. 6.— Spectropolarimetry of SN 2006my on day 38, plotted as 50 Å bins. The Stokes parameters have been rotated by  $174^\circ$ , as described in the text. The solid line in the top panel is the total flux spectrum. Note the high continuum polarization, near 1%, at continuum wavelengths near 7000 and 8000 Å. The two horizontal black bars mark our two continuum regions.

certainty of 0.04% in each Stokes parameter. Just as for SN 2006ov, the data for SN 2006my are consistent with negligible ISP in the host galaxy. In this object, the continuum polarization is distinctly lower than in SN 2006ov, although it is unclear how much of the difference is due to the later epoch of the SN 2006my observations.

### 3.3. SN 2007aa

Unlike the other two objects, SN 2007aa was discovered shortly after explosion, allowing us the opportunity to obtain data at early times and have a comparison for the late-time data.

Our first epoch of spectropolarimetry was obtained on day  $-50$ , well before the end of the plateau, and only 28 days after discovery. As discussed above, Folatelli & Morrell (2007) described a spectrum taken one day after discovery as being similar to that of SN 1999em at 20 days after explosion, implying an epoch for our first observation of  $\sim 47$  days after explosion. We used the SuperNova IDentification code of Blondin & Tonry (2007) to cross-correlate our day  $-50$

spectrum with a library of supernova templates, holding the redshift fixed. The top three individual SNe with spectral matches (ignoring spectra on multiple dates per object) were SNe 2004et, 2004dj, and 2006bp at 56, 56, and 58 days (respectively) after their estimated explosion dates (Sahu et al. 2006; Vinkó et al. 2006; Quimby et al. 2007).

These estimates are all consistent with SN 2007aa having a normal plateau duration of  $\sim 100$  days, with our first set of data being taken near the middle. Our second epoch, at day  $-22$ , was taken late in the plateau stage, but before the beginning of the steep decline phase, while our third epoch, on day 3, was taken during the steep decline and just before the beginning of the radioactive-decay tail.

The two plateau epochs of spectropolarimetry are plotted versus wavelength in Figure 7 and in the  $q-u$  plane in Figure 8. We have applied a rotation of  $172^\circ$  to the data in Figure 7 in anticipation of the late-time results. A low level of continuum polarization at early times in SN 2007aa is clear from Figure 7. At both epochs,  $u_{\text{RSP}}$  was near zero and  $q_{\text{RSP}}$  ranged over 0–0.2% in the continuum. Line polarization features are clearly present at the Balmer, Na I, Fe II, Ca II, and O I lines. The strongest line polarization feature, at  $\text{H}\alpha$ , had an extent of about 0.4% in the first epoch and grew to  $\sim 1\%$  in the second epoch. Close inspection of  $u_{\text{RSP}}$  in the second-epoch data shows small variations at the positions of the line features. This is a hint that the line features indicate deviations from axisymmetry.

To examine this in more detail, we have plotted the data points in the  $\text{H}\alpha$  line from day  $-22$  in Figure 8 as the solid black circles. The data points are 50 Å bins in wavelength from 6400 to 6750 Å, representing a velocity range of  $-7500$  to  $8400$   $\text{km s}^{-1}$  relative to  $\text{H}\alpha$ . The radius of each circle is proportional to wavelength, so the smaller points are in the blue wing of the profile and the larger circles are from the red wing. The  $\text{H}\alpha$  points show a spread in both  $q$  and  $u$  in a manner inconsistent with a simple axisymmetric geometry. In axisymmetry, all the points would lie along a line in  $q-u$  space. Instead, the points show a  $q-u$  “loop.” As one moves across the  $\text{H}\alpha$  profile from red to blue, one moves in a counterclockwise direction around the loop.

Such loops were first identified in supernova spectropolarimetry by Cropper et al. (1988) in the  $\text{H}\alpha$  and Ca II near-infrared (NIR) triplet lines of SN 1987A. The interpretation of the loops in SN 1987A has remained obscure for over 20 years despite the high quality of the data (Wang & Wheeler 2008). Subsequent investigations have found  $q-u$  loops in systems as different from SN 1987A as SNe IIn (Hoffman et al. 2008), stripped-envelope SNe (Maund et al. 2007a,b), and even SNe Ia (Kasen et al. 2003; Wang et al. 2003a; Chornock & Filippenko 2008). Kasen et al. (2003) found that loops were a generic consequence of systems containing multiple components with misaligned axes of symmetry and constructed a few examples with very different geometries. The relevance of these models to SN II atmospheres during the plateau stage is unclear as both the photosphere and  $\text{H}\alpha$ -forming region are within the hydrogen envelope of the progenitor. Chugai (1992) has a more promising model, specifically designed for SN 1987A, which interprets the  $\text{H}\alpha$  loops as evidence of a small number of individual clumps



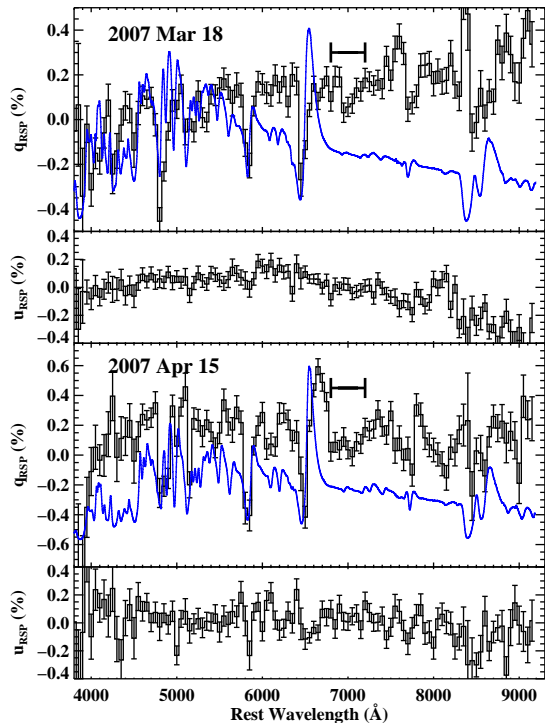


FIG. 7.— Early-time spectropolarimetry of SN 2007aa obtained while the object was on the plateau, on days  $-50$  and  $-22$ . The polarization data have been rotated by  $172^\circ.4$  to align  $q_{RSP}$  with the direction of the late-time continuum polarization. The blue solid lines in the background of each  $q_{RSP}$  plot are the total-flux spectra from each date. Note the weak continuum polarization with significant line polarization features. The “droop” in  $u_{RSP}$  to negative values in the 2007 March 18 polarization data at wavelengths greater than  $8200$  Å is unexplained and may not be real, although none of the standard or probe stars observed that night showed such an effect. In any case, none of the results presented in this paper rely on data from that portion of the spectrum. The horizontal black bar in each  $q_{RSP}$  panel marks our continuum region.

of  $^{56}\text{Ni}$  creating pockets of high ionization and  $\text{H}\alpha$  excitation. At different radial velocities, we see the effects of different clumps causing the net polarization angle to rotate with wavelength.

We defer additional analysis of the line polarization features in SN 2007aa to future work on the polarization of SNe II at early times because our focus here is on the continuum polarization and its temporal evolution. For now, we will note the following points. First, the long axis of the  $\text{H}\alpha$  loop on day  $-22$  is mostly aligned with the P.A. of the late-time continuum polarization, possibly indicating a common symmetry axis. Second, the total polarization excursion in the line is  $\sim 1\%$  at an epoch where the continuum polarization is likely to be very much lower, as discussed below.

We will now discuss the continuum polarization in detail. We found our low-S/N late-time polarization data in the final epoch to be unreliable near  $8100$  Å, so we have focused only on the bluer of our two continuum polarization windows,  $6800$ – $7200$  Å. Figure 8 has our continuum polarization measurements plotted for each of our three epochs of observation. As was clear from Figure 7, the observed continuum polarization on the plateau was very low. We measure formal polarizations of  $0.11 \pm 0.04\%$  and  $0.08 \pm 0.05\%$  on days  $-50$  and  $-22$ , respectively.

By contrast, the polarization after the end of the plateau jumped to  $0.83 \pm 0.12\%$  on day 3.

The late-time spectropolarimetry data of SN 2007aa from day 3 are plotted in Figure 9. The data are extremely noisy due to the faintness of the object at this time, but when binned up to  $100$  Å per pixel the basic appearance of the data is qualitatively similar to that shown previously for SN 2006ov and SN 2006my. The continuum polarization is near  $1\%$  in  $q_{RSP}$ , but there are broad dips down to near zero polarization at the locations of strong lines such as  $\text{H}\alpha$ , with  $u_{RSP}$  centered near zero. The polarization we measure at the peak of  $\text{H}\alpha$  is  $(q_{RSP}, u_{RSP}) = (0.02\%, 0.02\%)$ , with  $0.1\%$  error bars in each Stokes parameter, consistent with zero, as shown in Figure 8.

A few of the dips in polarization at the lines appear to reach negative values of  $q_{RSP}$ , especially near  $7650$  Å and  $8400$  Å, but these are only marginally statistically significant. The wavelength bins that are the most negative are those with the least flux from the SN (due to absorptions from the telluric A band and the Ca II NIR triplet P-Cygni feature) and hence the lowest S/N, magnifying any systematic uncertainties in the sky subtraction. An integration over  $8500$ – $8800$  Å, representing the emission component of the Ca II NIR triplet, gives  $(q_{RSP}, u_{RSP}) = (-0.09 \pm 0.17\%, -0.11 \pm 0.17\%)$ , which like the polarization at the peak of  $\text{H}\alpha$  is completely consistent with zero.

If we interpret the late-time polarization of SN 2007aa as being similar to that of SN 2006ov and SN 2006my, then the contribution from ISP should be low in this object as well, given the low polarization in the lines. Further evidence for this can be seen in Figure 8, where we have plotted the peaks of the  $\text{H}\alpha$  lines for all three epochs (integrated over the same  $6540$ – $6600$  Å interval). The  $\text{H}\alpha$  peaks in the first and last epoch are near zero. The  $\text{H}\alpha$  polarization in the second epoch is higher, but still low ( $0.3\%$ ). That is also the epoch showing clear evidence of strong polarization throughout the line, so perhaps a non-zero polarization at the peak is to be expected, particularly if an aspherical excitation distribution is present (Chugai 1992). Small amounts of ISP have a similar effect to changing the origin in the  $q$ – $u$  plane, so there is still a possibility of a pathological ISP canceling out some intrinsic supernova polarization. However, taken together with the low continuum polarization measured on the plateau, the simplest interpretation is that SN 2007aa, like SN 2006ov and SN 2006my, suffers minimal ISP ( $\lesssim 0.1\%$ ).

We have taken the continuum polarization measurements and plotted them versus time in Figure 10, along with the KAIT unfiltered light curve. The polarization shows a strong increase from the plateau stage to the late-time observations taken during the rapid decline phase. Even if we are mistaken about the ISP being negligible, the observation that there was a sharp change in the polarization associated with the end of the plateau is a robust result. This is strongly reminiscent of the jump in polarization seen in SN 2004dj (Leonard et al. 2006). In SN 2007aa, however, there was evidence of asphericity in the form of line polarization on the plateau, while SN 2004dj did not even show any line polarization features before the sudden increase in continuum polarization.



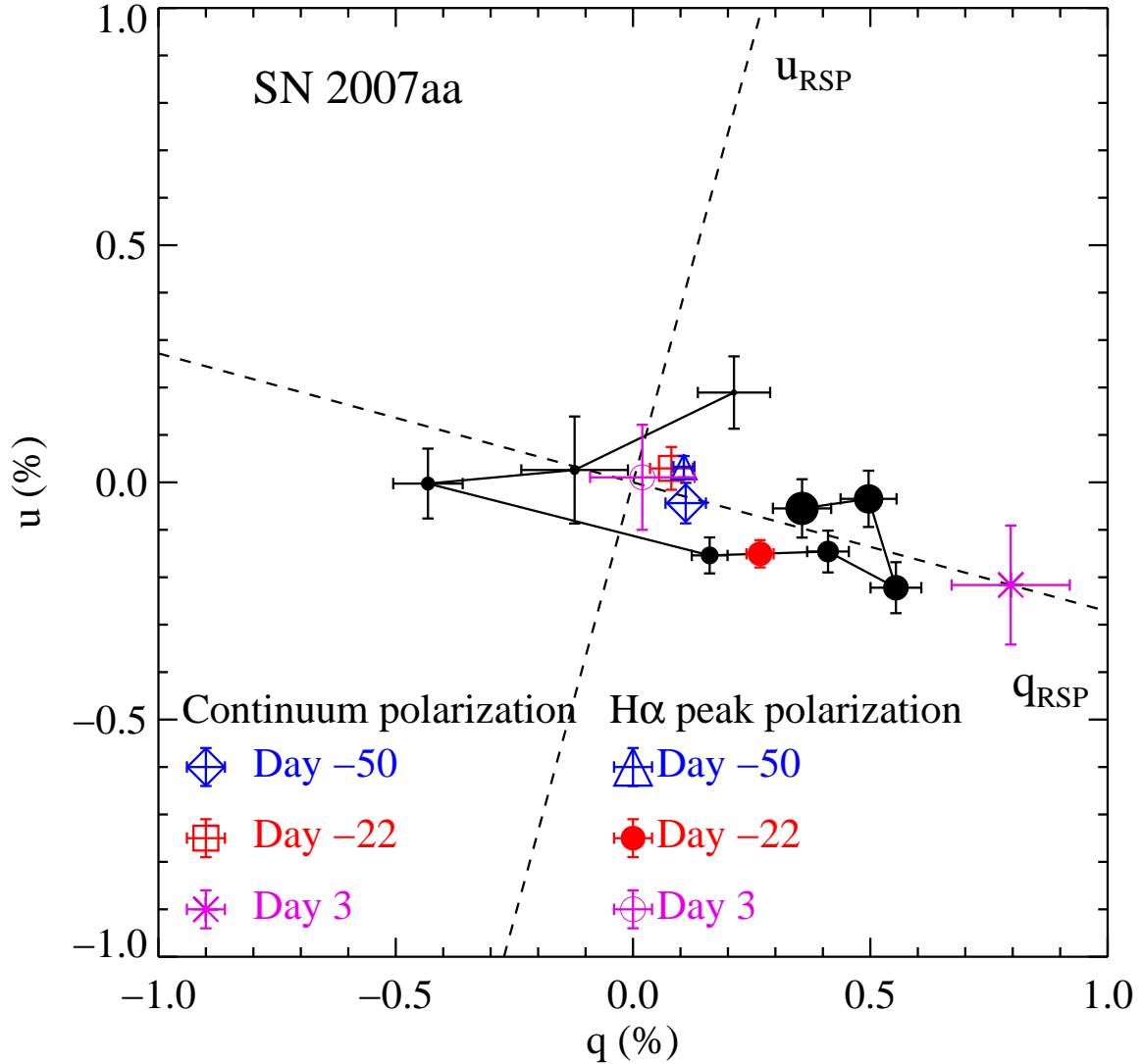


FIG. 8.— Polarization data for SN 2007aa plotted in the  $q-u$  plane. The solid black circles connected by a line are from the day  $-22$  data and are  $50 \text{ \AA}$  bins in wavelength from  $6400$  to  $6750 \text{ \AA}$ , representing a velocity range of  $-7500$  to  $8400 \text{ km s}^{-1}$  relative to  $\text{H}\alpha$ . The points form a loop in the  $q-u$  plane. The radius of each circle is proportional to wavelength, so moving across the line profile from blue to red corresponds to moving around the loop in a counterclockwise direction. Also plotted are continuum polarization points (integrations over  $6800\text{--}7200 \text{ \AA}$ ) and a set of points representing the peak of the  $\text{H}\alpha$  emission line (integrations over  $6540\text{--}6600 \text{ \AA}$ ). Note the low polarizations in the  $\text{H}\alpha$  peaks and in the continuum for the first two epochs, which together imply minimal ISP in this object. The day 3 continuum polarization represents a significant jump in polarization. The dashed lines represent the rotated  $q_{\text{RSP}}-u_{\text{RSP}}$  coordinate system, designed to have the  $q_{\text{RSP}}$  axis go through the day 3 continuum point.

#### 4. DISCUSSION

The spectropolarimetry data presented above for the three objects after the end of the plateau are all qualitatively similar with each other and with SN 2004dj (Leonard et al. 2006). The continuum polarization for each object is high, but flat and constant with wavelength between the strong line features in the red. This is a signature of the wavelength-independent nature of Thomson scattering. The lines produce large depolarizations and many overlapping lines significantly decrease the net polarization in the blue. The minimal polarizations at the peaks of  $\text{H}\alpha$  and lack of significant interstellar Na I absorptions are consistent with negligible ISP in all three objects, and therefore the large continuum polarizations are intrinsic to the SNe.

Classically, the expected effect of lines forming in front of an aspherical electron-scattering photosphere is to produce “inverse P-Cygni” line polarization features (Jeffery 1989). Line emission near zero velocity produces a dip in polarization near the line center, and selective blocking of forward-scattered light produces a polarization peak in the blueshifted absorption trough. Higher polarizations can also be found in the red wing of the line as the opaque photosphere obstructs the observer from seeing unpolarized line emission from the far side of the ejecta. This simple picture provides an explanation for the line polarization features in photospheric-phase spectropolarimetry of SN 1987A and SN 1999em (Jeffery 1991a,b; Leonard et al. 2001), and possibly our early data for SN 2007aa as well. However, we do not see emission peaks blueward of  $\text{H}\alpha$  or the Ca II NIR triplet in our

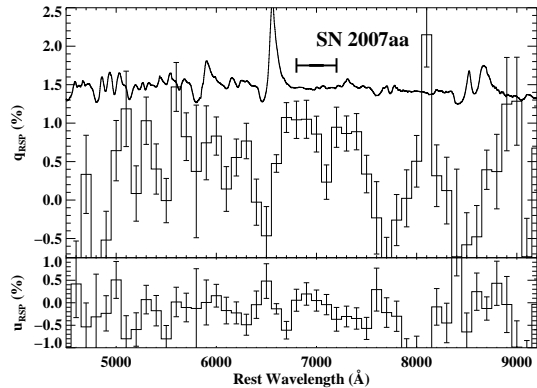


FIG. 9.— Late-time spectropolarimetry of SN 2007aa from day 3, presented in 100 Å bins. The solid line in the upper part of the top panel is the total-flux spectrum to guide the eye. High continuum polarization near 1% is seen in  $q_{RSP}$  with dips down near zero at the lines, while  $u_{RSP}$  is consistent with zero. The spike in  $q_{RSP}$  and dip in  $u_{RSP}$  near 8100 Å are spurious and are caused by systematically poor night-sky subtraction near that wavelength. The horizontal black bar marks our continuum region.

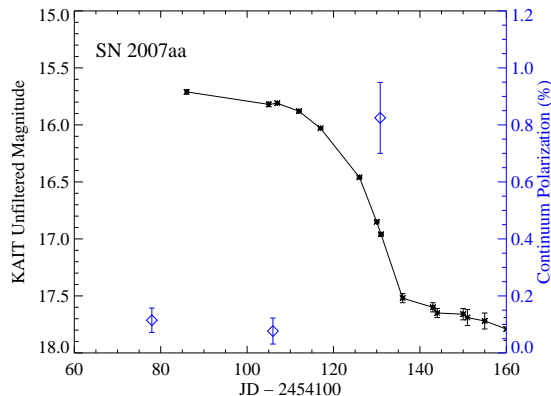


FIG. 10.— Time evolution of the continuum polarization of SN 2007aa compared to the KAIT unfiltered light curve (black stars connected by a line). The blue diamonds represent the continuum polarization integrated over 6800–7200 Å. The derived time of the end of the plateau,  $t_p$ , is JD = 2454227.8.

highest S/N late-time data (Fig. 3). Instead, the polarization is simply low relative to the continuum throughout the line profile. There are a few contributing effects.

The first is simple flux dilution. The continuum photosphere and associated polarizing electrons are located relatively deep in the supernova ejecta and intrinsically unpolarized line emission from the optically thin outer layers of the ejecta travels unimpeded to the observer and dilutes the observed polarization from the continuum value. As an example, the [Ca II]  $\lambda 7300$  doublet in the day 0 SN 2006ov data represents emission from the low-density parts of the outer ejecta. The line emission strengthens over time as the ejecta thin out and the supernova begins the transition to the nebular phase. This line has a flux peak a little less than a factor of  $\sim 2$  above the continuum (the continuum flux level is hard to define at this epoch because of many overlapping P-Cygni features), and the polarization dips from 1.3 – 1.4% in the nearby continuum pixels down to  $\sim 0.8\%$  in the line.

The second reason is that photons scattering in lines are generally depolarized (Höflich et al. 1996). While the outer layers of the ejecta are optically thin in the continuum, it seems likely that the optical depth in the strong

lines is still significant. The depolarizations over the full line profile from lines that are strong in the cool outer ejecta, such as Na I, Ca II, and H $\alpha$ , are likely manifestations of this effect. Absorption and reemission in the line causes the photons to lose the directional information previously imprinted upon them by electron scattering. The net effect of a large number of overlapping lines in the blue is to result in a decrease in polarization at those wavelengths (Howell et al. 2001). In addition, the line-formation region is very geometrically extended compared to the electron-scattering photosphere, so the selective blocking of forward-scattered light is not an important effect.

A few of the strong depolarizations do not correspond to obvious strong features in the total-flux spectrum. An example is the depolarization visible near 5700 Å in Figure 3, which was also present in SN 2004dj (Leonard et al. 2006). It is unclear which weak spectral feature is responsible for that depolarization and why the many other weak spectral features do not also result in similarly strong depolarizations.

The time evolution of the polarization is of significant interest. SNe IIP generally do not exhibit strong polarization shortly after explosion (Wang & Wheeler 2008), and yet SN 2004dj had a strong jump in continuum polarization near the end of its plateau (Leonard et al. 2006). The main motivation for this study was to determine whether SN 2004dj was unique, or if other SNe IIP exhibit similar polarization behavior. We have shown time-series plots for the two objects in our study with multipole polarimetry in Figures 5 and 10, but SN 2007aa was the only object with data taken on the plateau to establish the low early-time polarization.

To make further progress, we searched for SN IIP polarimetry in the literature. As discussed in §1, there are surprisingly few published datasets of SN IIP spectropolarimetry in the refereed literature. Since we are interested in the intrinsic continuum polarization, we must also exclude objects with large ISP corrections because estimates of ISP are uncertain and require making assumptions. SN 1999em (Leonard et al. 2001; Wang & Wheeler 2008) and SN 2004dj (Leonard et al. 2006) are the only objects from the published literature to meet our criteria. Of the three objects in the study by Leonard & Filippenko (2001), SNe 1997ds and 1999gi both had large and uncertain ISP contamination, and SN 1998A was a SN 1987A analog of unclear relevance to our SNe IIP. Leonard & Filippenko (2005) also plotted continuum polarization versus time for several SNe IIP, but three of the five objects in their sample had ISP corrections of 1% or more.

We collected photometry for the two objects from the literature and determined the date of the end of the plateau for each. The combined set of polarization versus time since  $t_p$  is shown in Figure 11. We must caution the reader that the data shown in this Figure are necessarily very heterogeneous.

We also reanalyzed the published polarization data in order to make our comparisons as uniform as possible. The published SN 1999em data generally do not extend sufficiently far to the red to include our favored continuum regions. We calculated the continuum polarization using as much of our 6800–7200 Å window as was available in each observation from the dataset of

Leonard et al. (2001). The 1999 Nov. 5 and 2000 Apr. 5/9 data included the full wavelength range, while for the 1999 Dec. 8 and 17 data we integrated from 6800 Å to the red wavelength end of the data. The 1999 Dec. 17 continuum polarization is the only one of the four values to differ from the synthesized *V*-band polarizations quoted by Leonard et al. (2001) by more than the error bars, possibly due to the limited wavelength range (the data from that night only extend redward to 6850 Å). The data have not been corrected for ISP because the effect is believed to be small ( $\sim 0.1\%$ ; Leonard et al. 2001).

As discussed above, applying the very wide continuum region used by Leonard et al. (2006) in their study of SN 2004dj to our SN 2006ov data would reduce the overall polarization measured on day 0 from 1.56% to 1.26%. To correct for this effect, we obtained the SN 2004dj data from D. Leonard and calculated the polarization in our two continuum windows in an identical manner to the other objects in this paper. Therefore, the peak continuum polarization plotted in Figure 11 is now 0.60%,  $\sim 10\%$  higher than the published value of 0.56% given by Leonard et al. (2006).

Despite these caveats, we believe the basic trend shown in Figure 11 is sound. At early times, SNe IIP are seen to exhibit low polarization (Wang & Wheeler 2008). The large, extended, slowly rotating hydrogen envelopes of their progenitors are unlikely to be substantially aspherical prior to explosion. Even an aspherical initial explosion will become more spherical when propagating outward through the remainder of the star (Chevalier & Soker 1989; Kifonidis et al. 2006). At the end of the plateau, the thick hydrogen envelope becomes mostly optically thin, allowing us to see deep into the ejecta and observe the aspherical core of the explosion. In addition, the observed polarization for a given geometry is expected to be maximized when the optical depth to electron scattering is nearly unity (e.g., Höflich 1991). To be fair, the dramatic jump in polarization was only directly seen in SN 2004dj and SN 2007aa. However, SN 2006ov does show a consistent increase in polarization of 0.3% in both of our continuum regions over the course of just five days, indicating very rapid changes in the continuum polarization.

It is instructive to compare to the supernova with the most densely sampled polarimetric data, SN 1987A. Jeffery (1991b) presented ISP-corrected broad-band polarimetry from a number of sources (Barrett 1988; Mendez et al. 1988). The *BVRI* polarizations do show a common trend of rising polarization at late times, with a possible spike in the *B* and *V* polarization percentages near the beginning of the radioactive-decay tail. While the SNe IIP in Figure 11 show declining polarization after the start of the radioactive tail, the SN 1987A data continue rising up to  $\sim 1\%$  at 200–300 days after explosion. The Type IIb SN 2001ig (Maund et al. 2007b) also showed a distinct jump in polarization associated with the hydrogen layer becoming optically thin and the photosphere receding into the He core.

Prior to the publication of the SN 2004dj polarization results, Chugai et al. (2005) noticed unusual line profiles present in that object in the nebular phase. The  $H\alpha$ ,  $H\beta$ , [O I], and [Ca II] lines all exhibited a double-

peaked structure with the main peak initially blueshifted by about  $1600 \text{ km s}^{-1}$  and moving redward with time, along with a similar peak on the red side of the profile. Chugai et al. (2005) modeled these line profiles in terms of a bipolar  $^{56}\text{Ni}$  component protruding from a more spherical “cocoon” that produced an ionization and excitation asymmetry. Chugai (2006) found that minimal adjustments to the initial model could roughly match the polarization results at the second nebular epoch, although his models did not predict the decline in polarization after the beginning of the radioactive-decay tail seen in the data or the different polarization angle seen in the first nebular dataset relative to the later data.

While asphericities in the  $^{56}\text{Ni}$  distribution are likely related to the polarization we observe in the three objects in our sample, none of them exhibits late-time line profiles similar to those of SN 2004dj. The late-time  $H\alpha$  profiles of our objects are shown in Figure 12. SNe 2006my and 2007aa have mostly rounded  $H\alpha$  profiles, with SN 2006my showing a small notch or dip near 6575 Å. The early-time spectra of SN 2006ov do show a pair of double notches, near 6535 Å and 6590 Å in the day  $-5$  spectrum, corresponding to velocities of  $-1250$  and  $1200 \text{ km s}^{-1}$  with respect to  $H\alpha$ . The notches disappeared in just five days and the line profiles after the end of the plateau were normal, by contrast with SN 2004dj, whose  $H\alpha$  line-profile asymmetries remained prominent for at least 330 days after explosion (Chugai et al. 2005). The blue and red notches in the  $H\alpha$  profile of SN 2006ov before the beginning of the radioactive-decay tail are reminiscent of the so-called “Bochum event” in SN 1987A (Hanuschik & Dachs 1987), although at significantly lower velocities ( $\sim 1200 \text{ km s}^{-1}$  versus  $\sim 4000 \text{ km s}^{-1}$  in SN 1987A). Similar notches have been seen in other SNe IIP near the end of the plateau (e.g., at  $v \approx 2500 \text{ km s}^{-1}$  in SN 1999em; Leonard et al. 2002a) and do likely indicate asphericities or clumps in the  $^{56}\text{Ni}$  distribution (Chugai 1992; Utrobin, Chugai, & Andronova 1995).

Given the evidence for a potentially clumpy  $^{56}\text{Ni}$  distribution, it is worth considering whether clumps of  $^{56}\text{Ni}$  or other deformations of the core-envelope boundary could be responsible for the continuum polarization that we measure, rather than an aspherical photosphere in the core. Leonard et al. (2006) hypothesized that the change in the polarization angle seen from the first to the second epoch after the end of the plateau in SN 2004dj was due to some non-axisymmetric portion of the  $^{56}\text{Ni}$  distribution beginning to be uncovered before the whole core as the photosphere receded in the ejecta. Chugai (2006) proposed an alternative explanation, which he termed a “spotty photosphere,” invoking an inhomogeneous distribution of the elements at the hydrogen-helium boundary due to fluid instabilities at that interface during the explosion (Müller et al. 1991). These inhomogeneities would result in brightness and opacity variations that would be manifested as a nonzero net polarization that suddenly appears when the overlying layers become optically thin and the photosphere passes through the core-envelope boundary, even if the core of the SN were essentially spherical on large scales.

Our data for these three objects do not show any angle variations of the type seen in SN 2004dj. The polarization angles for SN 2006ov are identical for all three

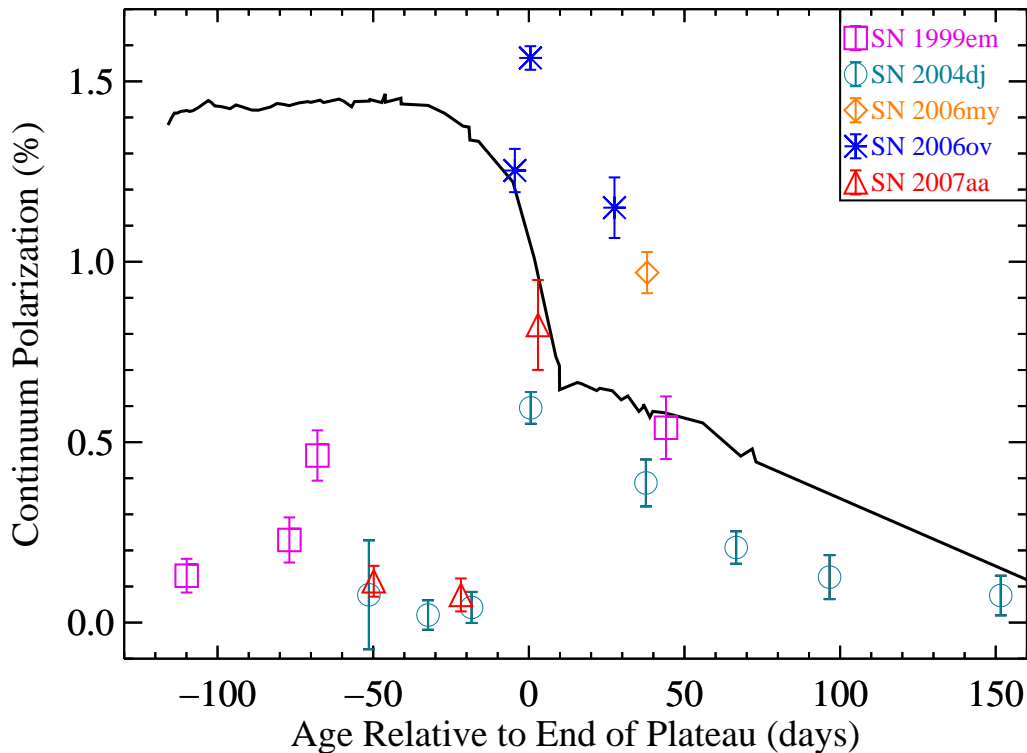


FIG. 11.— Compilation of SN IIP intrinsic continuum polarization measurements after correction for ISP. The SN 1999em data (purple squares) are from Leonard et al. (2001) and the SN 2004dj data (cyan circles) are from Leonard et al. (2006), reanalyzed in a manner similar to the current objects (see text for details). The SNe 2006ov (blue stars), 2006my (orange diamond), and 2007aa (red triangles) data points are from this work. The abscissa represents time in days relative to the end of the plateau,  $t_p$ , for each object, as defined in the text. We used  $R$ -band photometry from Leonard et al. (2006) and Vinkó et al. (2006) to derive  $t_p$  for SN 2004dj of 2004 Oct. 12.4, and  $R$ -band photometry from Leonard et al. (2002a) and Hamuy et al. (2001) were used to derive  $t_p$  for SN 1999em of 2000 Feb 23.3. A systematic error contribution of 0.04% has been added in quadrature to all points to account for potential night-to-night instrumental variations, except for the SN 2004dj data, which already included a systematic error contribution. The black solid line is the well-sampled  $R$ -band light curve of SN 1999em to guide the eye. The data are consistent with a sharp increase in the continuum polarization in the last 10–20 days before the end of the plateau.

epochs from day  $-5$  through day 27. While the continuum polarization for SN 2007aa at early times is sufficiently small that the polarization angle is hard to reliably measure (a small amount of ISP could result in dramatic changes in the inferred angle), the long axis of the  $q - u$  loop seen in the  $H\alpha$  line on day  $-22$  (Fig. 8) is approximately aligned with the late-time continuum polarization. The combination of low continuum polarization and significant line polarization (as seen in day  $-22$  in SN 2007aa) may indicate that the  $H\alpha$  excitation is more sensitive to the underlying aspherical  $^{56}\text{Ni}$  distribution than the continuum and hence the alignment with the late-time polarization is not accidental. In addition, the continuum polarization in SN 1999em remained at a constant P.A. over the course of the first 161 days after explosion (Leonard et al. 2001). The polarization angle variation of SN 2004dj appears to be an outlier compared to these other objects, or else the first observation after the end of the plateau was very fortunately timed to catch the polarization angle while it was rapidly varying.

The simplest explanation for the constancy of the polarization angles is that these SNe IIP have highly aspherical cores surrounded by hydrogen envelopes that are more spherical. Thus, we conclude that our late-time continuum polarization measurements are most easily

understood as good tracers of the underlying asphericity of the photosphere in the core, and not of a “spotty photosphere” or other boundary effect that only produces a transient polarization signal when the photosphere enters the core. Observations taken well before the photosphere recedes through the boundary between the hydrogen-rich envelope and the helium-rich core already show signs of the asphericity that is present at late times.

Our maximum continuum polarization of 1.56% in SN 2006ov on day 0 implies a minimum axis ratio of 1.45:1 in the context of the aspherical electron-scattering atmospheres of Höflich (1991), if the object were viewed in the equatorial plane, and possibly higher if the symmetry axis were less inclined to the line of sight. Despite the lower continuum polarization observed in SN 2004dj, Leonard et al. (2006) derived a similar axis ratio for the core of that object after accounting for the preferred inclination of Chugai et al. (2005).

SN 2006ov also shows some evidence for inner asphericity in the late-time [O I] line profiles. The profiles of the  $\lambda\lambda 6300, 6364$  doublet in our latest spectrum (day 51) are shown in Figure 13. Although the spectrum has not yet become fully nebular and the [O I] doublet does not yet completely dominate its portion of the spectrum, a double-peaked structure is apparent. The peaks in  $\lambda 6300$  are at velocities near 0 and  $850 \text{ km s}^{-1}$ . Confirmation

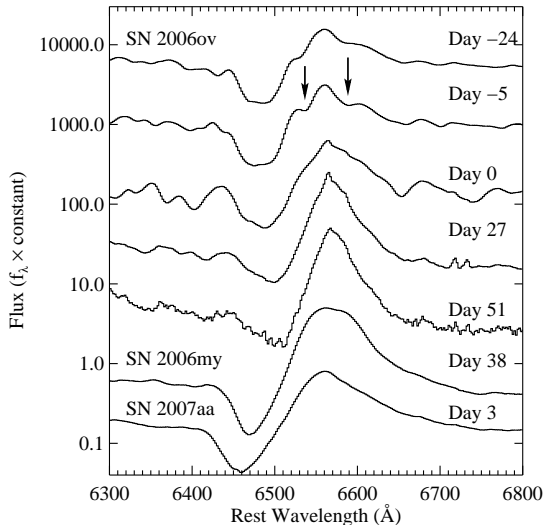


FIG. 12.— Late-time  $H\alpha$  line profiles. The spectra are labeled by their ages relative to  $t_p$ . The bottom two spectra are of SN 2006my and 2007aa, while the remainder are of SN 2006ov. The day  $-24$  spectrum of SN 2006ov is from Li et al. (2007), while the day 51 spectrum was acquired on 2007 Feb. 14.655 with LRIS using a setup similar to that for the other spectra. Two notches (marked with arrows) are seen in the earliest SN 2006ov spectra near 6535 and 6590 Å. At later times, none of the objects shows significant asymmetries in the  $H\alpha$  line profile.

that this represents the oxygen distribution and not contamination by some other line can be seen from the profile of  $\lambda 6364$ , which shows a peak near zero velocity as well as one to the red; however, the redder peak in  $\lambda 6364$  is closer to  $500 \text{ km s}^{-1}$ .

Double-peaked [O I] profiles have been seen in stripped-envelope supernovae and attributed to a toroidal oxygen distribution (Mazzali et al. 2005; Maeda et al. 2008; Modjaz et al. 2008), but the velocity splittings of the peaks in those objects are significantly higher. Alternative geometries are also possible (Taubenberger et al. 2009; Milisavljevic et al. 2010). Here, a more likely explanation is that we are seeing large-scale clumps or blobs in the inner oxygen distribution, especially given that the main peak is at zero velocity. Such oxygen clumps have been seen in stripped-envelope supernovae (Filippenko & Sargent 1989; Matheson et al. 2000; Silverman et al. 2009), SN 1987A (Stathakis et al. 1991), and the SN IIP 2002hh (Pozzo et al. 2006). The clumps are usually attributed to Rayleigh-Taylor instabilities created at the interface of the oxygen-rich and helium-rich layers in the core during the explosion (Müller et al. 1991), although other large-scale fluid motions during the explosion are possible.

## 5. CONCLUSIONS

We have presented late-time spectropolarimetry of three SNe IIP. All three objects had large continuum polarizations after the end of the photometric plateau ( $0.8 \lesssim P \lesssim 1.6\%$ ), while SN 2007aa had contrastingly smaller continuum polarization on the plateau ( $P \approx 0.1\%$ ). These results confirm that the polarization evolution of SN 2004dj (Leonard et al. 2006) was not unique and that highly aspherical cores exist in SNe IIP. This follows the trend identified by Wang et al. (2001) that the degree of polarization in core-collapse SNe generally

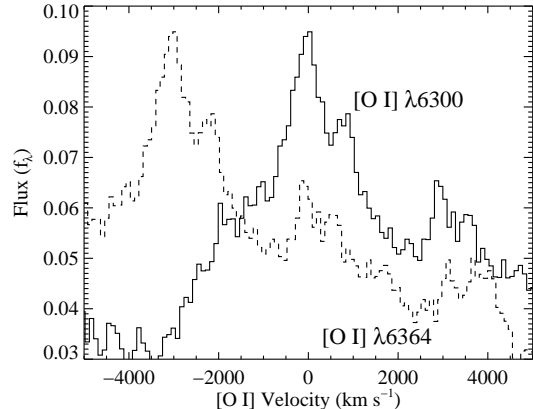


FIG. 13.— Late-time [O I] line profiles in SN 2006ov from day 51. The solid line shows velocities relative to  $\lambda 6300$  and the dashed line shows velocities relative to the  $\lambda 6364$  component of the doublet. Two peaks are observed in both, near 0 and  $850 \text{ km s}^{-1}$  for  $\lambda 6300$ . These are likely a sign of large-scale clumps in the oxygen-rich inner core, perhaps as a result of Rayleigh-Taylor instabilities in the explosion.

increases with time.

It is important to note that an intrinsic continuum polarization of 1.56% is quite high<sup>5</sup>. Although there are extreme cases such as the SN Ic 1997X (Wang et al. 2001), very few core-collapse SNe exhibit intrinsic continuum polarizations higher than this. Most stripped-envelope SNe have significantly lower continuum polarization (after correction for ISP), including even extreme examples such as the well-studied broad-lined SN Ic 2002ap (Kawabata et al. 2002; Leonard et al. 2002b; Wang et al. 2003b). The line polarization features in some objects are stronger, however. SNe IIP are the single most common form of core-collapse supernova and represent the explosions of the most common massive stars, those at the low-mass end of the range of supernova progenitors. Our observations of these objects demonstrate that large degrees of asphericity are generic ingredients in even ordinary core-collapse explosions and are not just limited to various unusual or extreme objects.

This observational view parallels recent developments in the theoretical modeling of core-collapse SNe. Modern simulations of supernova explosions have revealed a rich phenomenology of multi-dimensional effects (Blondin et al. 2003; Burrows et al. 2006). Extreme models invoking jets (Khokhlov et al. 1999) have had some success explaining the polarization evolution and other tracers of asphericity in core-collapse SNe (Höflich et al. 2001; Couch et al. 2009), although the mechanism by which jets would be launched in ordinary SNe IIP remains obscure, as jet formation is usually thought to require atypically high angular momentum in the core (e.g., Burrows et al. 2007b). Moreover, the current generation of neutrino-powered core-collapse simulations (e.g., Blondin & Mezzacappa 2007; Burrows et al. 2007a; Marek & Janka 2009) all generate complex structures in the explosion without needing to invoke jets. In particular, these simulations commonly create aspherical shocks dominated by low-order deformations that produce unipolar or bipolar outflows that seem promising for generating the core asphericities we

<sup>5</sup> We caution that the precise polarization value is dependent on the definition of the continuum regions.

infer from our polarization measurements. It remains to be seen whether these features persist in the upcoming more-detailed three-dimensional models.

Unfortunately, most explosion models to date only simulate the central core of the star and stop when an outward-going shock is launched (or has failed to launch). However, the shock continues to evolve as it traverses the star and our observations can only probe the final state of the core, which makes detailed comparisons of the observed asphericities to those seen in the simulations difficult. Only a few studies (Kifonidis et al. 2006; Hammer et al. 2009) have followed the aspherical shock wave as it propagates outward through the star. Future work in this direction, along with radiative-transfer calculations, is necessary to see if the existing models can reproduce the observations.

It is interesting to note that SN 2006ov showed the largest continuum polarizations in our sample while it ejected the smallest amount of nickel and possibly had the lowest-mass progenitor. As mentioned above, Smartt et al. (2009) quote a  $^{56}\text{Ni}$  mass of  $0.003 \pm 0.002 M_{\odot}$ , a value about an order of magnitude lower than in most SNe IIP. That SN 2006ov ejected a low  $^{56}\text{Ni}$  mass can also be inferred by comparison of Figures 5 and 10. SN 2006ov and SN 2007aa had similar magnitudes on the plateau and SN 2006ov was at a somewhat smaller distance (Smartt et al. 2009), yet it was a magnitude fainter than SN 2007aa at the beginning of the radioactive decay tail. The progenitor mass limit for SN 2006ov is also very low,  $M < 10 M_{\odot}$  (Smartt et al. 2009; Crockett et al. 2009). In addition, the expansion velocities of SN 2006ov are lower than those of the other SNe IIP (Figure 12), possibly indicating a low explosion energy. A connection between the low nickel mass, low progenitor mass, or low explosion energy and the high continuum polarization would be exciting if confirmed in other objects.

We also encourage the enlargement of the published SN IIP spectropolarimetry sample, particularly of ob-

jects lacking significant ISP. While observations at very late times are likely rare in the extant unpublished datasets, it would be fruitful to expand the number of objects plotted in Figure 11. Only then will we be able to look for relationships between the core asphericity and other supernova properties. Trends with progenitor mass, explosion energy, and  $^{56}\text{Ni}$  production will all be interesting to examine and may provide constraints on the theoretical uncertainties in the core-collapse supernova mechanism.

We thank Douglas C. Leonard for supplying us with his SNe 1999em and 2004dj data and Ryan J. Foley, Mohan Ganeshalingam, Matthew Moore, and Thea N. Steele for their assistance with some of the observations. Most of the data presented herein were obtained at the W. M. Keck Observatory, which is operated as a scientific partnership among the California Institute of Technology, the University of California, and the National Aeronautics and Space Administration; it was made possible by the generous financial support of the W. M. Keck Foundation. The authors wish to recognize and acknowledge the very significant cultural role and reverence that the summit of Mauna Kea has always had within the indigenous Hawaiian community; we are most fortunate to have the opportunity to conduct observations from this mountain. We also would like to thank the expert assistance of the Keck and Lick staffs in making these observations possible. A.V.F.'s supernova group at U.C. Berkeley has been supported by NSF grants AST-0607485 and AST-0908886, as well as by the TABASGO Foundation. KAIT and its ongoing operation were made possible by donations from Sun Microsystems, Inc., the Hewlett-Packard Company, AutoScope Corporation, Lick Observatory, the NSF, the University of California, the Sylvia & Jim Katzman Foundation, and the TABASGO Foundation.

*Facilities:* Shane (Kast), Keck:I (LRIS)

#### REFERENCES

- Barbon, R., Ciatti, F., & Rosino, L. 1979, *A&A*, 72, 287  
 Barrett, P. 1988, *MNRAS*, 234, 937  
 Berdyugin, A., Snåre, M.-O., & Teerikorpi, P. 1995, *A&A*, 294, 568  
 Blondin, J. M., & Mezzacappa, A. 2007, *Nature*, 445, 58  
 Blondin, J. M., Mezzacappa, A., & DeMarino, C. 2003, *ApJ*, 584, 971  
 Blondin, S., Modjaz, M., Kirshner, R., & Challis, P. 2006, *Central Bureau Electronic Telegrams*, 757  
 Blondin, S., & Tonry, J. L. 2007, *ApJ*, 666, 1024  
 Burrows, A., Dessart, L., Livne, E., Ott, C. D., & Murphy, J. 2007b, *ApJ*, 664, 416  
 Burrows, A., Livne, E., Dessart, L., Ott, C. D., & Murphy, J. 2006, *ApJ*, 640, 878  
 Burrows, A., Livne, E., Dessart, L., Ott, C. D., & Murphy, J. 2007a, *ApJ*, 655, 416  
 Chevalier, R. A., & Soker, N. 1989, *ApJ*, 341, 867  
 Chornock, R., & Filippenko, A. V. 2008, *AJ*, 136, 2227  
 Chugai, N. N. 1992, *Soviet Astron. Lett.*, 18, 168  
 Chugai, N. N. 2006, *Astron. Lett.*, 32, 739  
 Chugai, N. N., Fabrika, S. N., Sholukhova, S. N., Goranskij, V. P., Abolmasov, P. K., & Vlasyuk, V. V. 2005, *Astronomy Letters*, 31, 792  
 Clemens, D. P., & Tapia, S. 1990, *PASP*, 102, 179  
 Crockett, R. M., Smartt, S. J., Pastorello, A., Stephens, A. W., Maund, J. R., & Mattila, S. 2009, *arXiv:0912.3302*  
 Cropper, M., Bailey, J., McCowage, J., Cannon, R. D., & Couch, W. J. 1988, *MNRAS*, 231, 695  
 Couch, S. M., Wheeler, J. C., & Milosavljević, M. 2009, *ApJ*, 696, 953  
 Doggett, J. B., & Branch, D. 1985, *ApJ*, 90, 2303  
 Doi, T. 2007, *Central Bureau Electronic Telegrams*, 848  
 Eastman, R. G., Woosley, S. E., Weaver, T. A., & Pinto, P. A. 1994, *ApJ*, 430, 300  
 Fesen, R. A. 2001, *ApJS*, 133, 161  
 Filippenko, A. V. 1982, *PASP*, 94, 715  
 Filippenko, A. V., Li, W., Treffers, R. R., & Modjaz, M. 2001, in *Small-Telescope Astronomy on Global Scales*, ed. W.-P. Chen, C. Lemme, & B. Paczyński (ASP Conf. Ser. 246; San Francisco: ASP), 121  
 Filippenko, A. V., & Sargent, W. L. W. 1989, *ApJ*, 345, L43  
 Folatelli, G., & Morrell, N. 2007, *Central Bureau Electronic Telegrams*, 850  
 Hammer, N. J., Janka, H.-Th., & Müller, E. 2009, *ApJ*, submitted, *arXiv:0908.3474*  
 Hamuy, M. 2003, *ApJ*, 582, 905  
 Hamuy, M., et al. 2001, *ApJ*, 558, 615  
 Hanuschik, R. W., & Dachs, J. 1987, *A&A*, 182, L29  
 Heger, A., Fryer, C. L., Woosley, S. E., Langer, N., & Hartmann, D. H. 2003, *ApJ*, 591, 288  
 Hoffman, J. L., Leonard, D. C., Chornock, R., Filippenko, A. V., Barth, A. J., & Matheson, T. 2008, *ApJ*, 688, 1186  
 Höflich, P. 1991, *A&A*, 246, 481  
 Höflich, P., Khokhlov, A., & Wang, L. 2001, in *Proc. 20th Texas Symposium of Relativistic Astrophysics*, ed. J. C. Wheeler, H. Martel, (New York: AIP), 459



- Höflich, P., Wheeler, J. C., Hines, D. C., & Trammell, S. R. 1996, *ApJ*, 459, 307
- Horne, K. 1986, *PASP*, 98, 609
- Howell, D. A., Höflich, P., Wang, L., & Wheeler, J. C. 2001, *ApJ*, 556, 302
- Jeffery, D. J. 1989, *ApJS*, 71, 951
- Jeffery, D. J. 1991a, *ApJ*, 375, 264
- Jeffery, D. J. 1991b, *ApJS*, 77, 405
- Kasen, D., & Woosley, S. E. 2009, *ApJ*, 703, 2205
- Kasen, D., et al. 2003, *ApJ*, 593, 788
- Kawabata, K., et al. 2002, *ApJ*, 580, L39
- Khokhlov, A. M., Höflich, P. A., Oran, E. S., Wheeler, J. C., Wang, L., & Chtchelkanova, A. Yu. 1999, *ApJ*, 524, L107
- Kifonidis, K., Plewa, T., Scheck, L., Janka, H.-Th., & Müller, E. 2006, *A&A*, 453, 661
- Leonard, D. C., & Filippenko, A. V. 2001, *PASP*, 113, 920
- Leonard, D. C., & Filippenko, A. V. 2005, in *1604–2004: Supernovae as Cosmological Lighthouses*, ed. M. Turatto, et al. (San Francisco: ASP), 342, 330
- Leonard, D. C., Filippenko, A. V., Ardila, D. R., & Brotherton, M. S. 2001, *ApJ*, 553, 861
- Leonard, D. C., Filippenko, A. V., Chornock, R., & Foley, R. J. 2002b, *PASP*, 114, 1333
- Leonard, D. C., Gal-Yam, A., Fox, D. B., Cameron, P. B., Johansson, E. M., Kraus, A. L., Le Mignant, D., van Dam, M. A. 2009, *PASP*, 120, 1259
- Leonard, D. C., et al. 2002a, *PASP*, 114, 35
- Leonard, D. C., et al. 2006, *Nature*, 440, 505
- Li, W., Filippenko, A. V., Chornock, R., & Jha, S. 2003, *PASP*, 115, 844
- Li, W., Van Dyk, S., Filippenko, A. V., Cuillandre, J.-C., Jha, S., Bloom, J. S., Riess, A. G., Livio, M. 2006, *ApJ*, 641, 1060
- Li, W., Wang, X., Van Dyk, S. D., Cuillandre, J.-C., Foley, R. J., & Filippenko, A. V. 2007, *ApJ*, 661, 1013
- Lyne, D. A., & Lorimer, D. R. 1994, *Nature*, 369, 127
- Maeda, K., et al. 2008, *Science*, 319, 1220
- Marek, A., & Janka, H.-Th. 2009, *ApJ*, 694, 664
- Matheson, T., Filippenko, A. V., Ho, L. C., Barth, A. J., & Leonard, D. C. 2000, *AJ*, 120, 1499
- Mathewson, D. S., & Ford, V. L. 1970, *MmRAS*, 74, 139
- Maund, J. R., Wheeler, J. C., Patat, F., Baade, D., Wang, L., & Höflich, P. A. 2007a, *MNRAS*, 381, 201
- Maund, J. R., Wheeler, J. C., Patat, F., Wang, L., Baade, D., & Höflich, P. A. 2007b, *ApJ*, 671, 1944
- Mazzali, P., et al. 2005, *Science*, 308, 1284
- Mendez, M., Clocchiatti, A., Benvenuto, O. G., Feinstein, C., & Marraco, H. G. 1988, *ApJ*, 334, 295
- Milislavljivic, D., Fesen, R., Gerardy, C., Kirshner, R., & Challis, P. 2010, *ApJ*, 709, 1343
- Miller, J. S., Robinson, L. B., & Goodrich, R. W. 1988, in *Instrumentation for Ground-Based Astronomy*, ed. L. B. Robinson (New York: Springer-Verlag), 157
- Miller, J. S., & Stone, R. P. S. 1993, *Lick Observatory Technical Reports*, 66 (Santa Cruz, CA: Lick Obs.)
- Modjaz, M., Kirshner, R. P., Blondin, S., Challis, P., Matheson, T. 2008, *ApJ*, 687, L9
- Müller, E., Fryxell, B., & Arnett, D. 1991, *A&A*, 251, 505
- Munari, U., & Zwitter, T. 1997, *A&A*, 318, 269
- Nakano, S. & Itagaki, K. 2006a, Central Bureau Electronic Telegrams, 727
- Nakano, S. & Itagaki, K. 2006b, Central Bureau Electronic Telegrams, 756
- Oke, J. B., et al. 1995, *PASP*, 107, 375
- Pastorello, A., et al. 2004, *MNRAS*, 347, 74
- Poznanski, D., et al. 2009, *ApJ*, 694, 1067
- Pozzo, M., et al. 2006, 368, 1169
- Quimby, R. M., Wheeler, J. C., Höflich, P., Akerlof, C. W., Brown, P. J., & Rykoff, E. S. 2007, *ApJ*, 666, 1093
- Sahu, D. K., Anupama, G. C., Srividya, S., & Muneer, S. 2006, *MNRAS*, 372, 1315
- Schlegel, D. J., Finkbeiner, D. P., & Davis, M. 1998, *ApJ*, 500, 525
- Schmidt, G. D., Elston, R., & Lupie, O. L. 1992, *AJ*, 104, 1563
- Serkowski, K., Mathewson, D. S., & Ford, V. L. 1975, *ApJ*, 196, 261
- Shapiro, P. R., & Sutherland, P. G. 1982, *ApJ*, 263, 902
- Silverman, J. M., Mazzali, P., Chornock, R., Filippenko, A. V., Clocchiatti, A., Phillips, M. M., Ganeshalingam, M., & Foley, R. J. 2009, *PASP*, 121, 689
- Smartt, S. J., Eldridge, J. J., Crockett, R. M., & Maund, J. 2009, *MNRAS*, 395, 1409
- Stanishev, V. & Nielsen, T. B. 2006, Central Bureau Electronic Telegrams, 737
- Stathakis, R. A., Dopita, M. A., Cannon, R. D., & Sadler, E. M. 1991, in *Supernovae: The Tenth Santa Cruz Workshop in Astronomy and Astrophysics*, ed. S. Woosley (New York: Springer Verlag), 95
- Stetson, P. B. 1987, *PASP*, 99, 191
- Taubenberger, S., et al. 2009, *MNRAS*, 397, 677
- Trammell, S. R., Dinerstein, H. L., & Goodrich, R. W. 1993a, *ApJ*, 402, 249
- Trammell, S. R., Hines, D. C., & Wheeler, J. C. 1993b, *ApJ*, 414, L21
- Tran, H. D. 1995a, *ApJ*, 440, 565
- Tran, H. D. 1995b, *ApJ*, 440, 578
- Tran, H. D., Filippenko, A. V., Schmidt, G. D., Bjorkman, K. S., Jannuzi, B., & Smith, P. S. 1997, *PASP*, 109, 489
- Utrobin, V. P., Chugai, N. N., & Andronova, A. A. 1995, *A&A*, 295, 129
- Vinkó, J, et al. 2006, *MNRAS*, 369, 1780
- Wade, R. A. & Horne, K. 1988, *ApJ*, 324, 411
- Wang, L., Baade, D., Höflich, P., & Wheeler, J. C. 2003b, *ApJ*, 592, 457
- Wang, L., Howell, D. A., Höflich, P., & Wheeler, J. C. 2001, *ApJ*, 550, 1030
- Wang, L., & Wheeler, J. C. 2008, *ARA&A*, 46, 433
- Wang, L., et al. 2002, *ApJ*, 579, 671
- Wang, L., et al. 2003a, *ApJ*, 591, 1110